word count: 10270

Revision #2

Effects of electronegativities and charge delocalization on Q^2 Raman shifts of alkaline- and alkaline earth-bearing glasses and metasilicate crystals

Nesbitt, H. Wayne*[1], Dean, Phil A.W.[2], Bancroft, G.Michael[2], Henderson, Grant S.[3],

[1]Dept. of Earth Sciences, Univ. of Western Ontario, London, Ont. Canada

[2]Dept. of Chemistry, Univ. of Western Ontario, London, Ont. Canada

[3]Dept. of Earth Science, Univ. of Toronto, Toronto, Ont. Canada

Key words: Raman spectroscopy; electronegativity Charge delocalization in silicates; tetrahedral symmetric stretch, silicate glasses

Corresponding Author: H. Wayne Nesbitt: e-mail: hwn@uwo.ca

ABSTRACT

Raman shifts of the symmetric stretch of silicate Q^2 species vary over a range of ~90 cm^{-1} in crystals and glasses containing alkali and alkaline earth oxides. The shifts display a striking, sympathetic relationship with the electronegativity of the alkali and alkaline earths metals (M) with highest frequency observed for Mg-silicate glasses and crystals and the lowest frequency for Cs-bearing glasses. Frequencies are determined primarily by the electron density on constituent Si and O atoms of the Q^2 tetrahedra, as measured by Si 2p and O 1s X-ray Photoelectron Spectra (XPS). The electron density is, in turn, determined by the extent to which electronic charge is transferred from the modifier metal 'M' to the NBO of the Q^2 tetrahedron. The charge transferred to NBO is redistributed (delocalized) over all atoms of the tetrahedron by the four equivalent Si sp^3 orbitals. Although negative charge accumulates on all atoms of the tetrahedron, it accumulates preferentially on Si. Coulombic interactions among Si and all O atoms are thus weakened resulting in decreased force constants and lowered symmetric stretch frequencies of Q^2 species.

Density functional theoretical (DFT) calculations on six staggered and eclipsed $M_6Si_2O_7$ (M=Li, Na, K) molecules corroborate the findings. Charge is transferred from the metal atoms to NBO and delocalized over tetrahedra in accordance with Li, Na and K electronegativities. Calculated Si-O force constants and Raman shifts decrease with decreasing electronegativity of the cation but surprisingly, calculated Si-NBO bond lengths are largely unaffected, with all being similar at 1.665 ± 0.003 Å.

INTRODUCTION

Silicate crystals, glasses and melts incorporating alkalis and alkaline earths (M atoms) are partly covalently bonded (sp^3 hybridized Si-O bonds) and partly ionically bonded (M-O bonds).

Study of the molecular and ionic components consequently requires techniques sensitive to the properties of each type of contribution. Raman spectroscopy is sensitive to vibrational properties of silicate tetrahedra such as the frequency of the symmetric stretch and it has been used routinely to determine the presence and abundance of the various types of Si tetrahedra in these phases (e.g., Brawer and White, 1975; Furukawa et al., 1981; Mysen et al., 1982; Matson et al., 1983; McMillan, 1984; Chopelas, 1991; 1999; Mysen and Frantz, 1992; 1993; Frantz and Mysen, 1995; Richet et al., 1996; 1998; Choudhury et al., 1998; Wang et al., 2001; Neuville, 2006; Nasikas et al. 2011; Nesbitt et al. 2018; 2019; 2021; Bancroft et al. 2018; O'Shaughnessy et al. 2020; Moulton et al., 2021). Raman spectroscopic results pertinent to metasilicate crystals and glasses of near-metasilicate composition, are the focus of the study, with particular emphasis placed on understanding the processes affecting the symmetric stretch of SiO_4 tetrahedra in these phases.

Si tetrahedra are commonly described in terms of Q^n species where the central Si is bonded either to bridging oxygen (BO or Si-O-Si moieties) or to non-bridging oxygen (NBO or Si-O-M moieties). The superscript 'n' represents the number of BO atoms bonded to a Si center. The symmetric stretch of Q species is located in the region between ~800 cm^{-1} and ~1250 cm^{-1} of Raman spectra and there is general acceptance that Raman shifts decrease in a regular, stepwise manner from Q^4 to Q^0 in alkali and alkaline earth glasses and crystals: ~1200 cm^{-2} for Q^4; 1050-1100 cm^{-1} for Q^3; 950-1000 cm^{-1} for Q^2; ~900 cm^{-1} for Q^1; and ~850 cm^{-1} for Q^0 (Brawer and White, 1975; McMillan, 1984; Bancroft et al., 2018). Calculations on simple crystalline "structural units" are qualitatively consistent with this trend (Furukawa et al. 1981). Evidence presented here demonstrates that the Q^2 species symmetric stretch spans a much greater range than previously considered, and that its frequency depends strongly on the type of

counter cation (M) present in the crystal or glass. The large range of frequencies observed (Tables 1, 2) has been neither previously discussed nor explained, perhaps because, as noted by McMillan (1984) and Williams and Cooney (1992), there has been "neglect of M-O interactions" and their effect on Raman shifts. To address this aspect, we use Raman and XPS spectroscopic results from the literature and ab-initio (DFT) calculations on model $M_6Si_2O_7$ "species" to investigate the properties affecting or controlling the frequencies of the Q^2 symmetric stretch of metasilicate crystals and glasses. The findings have important implications related to verification of calculations of glasses and melts.

BACKGROUND

Characteristic and proxy frequencies

The relationship among vibrational frequency (ν), force constant (k) and reduced mass (μ) of a harmonic oscillator is (Moelwyn-Hughes, 1964):

$$\nu = (a/2\pi)\sqrt{(k/\mu)} \quad (1)$$

The proportionality constant 'a' is 1 where units are N/m and 25.89 for dynes/cm. The symmetric stretch of Q^2 species of crystals and glasses is determined by 'μ' and 'k' of the Si-O oscillators of tetrahedra. The characteristic vibrational frequency of the symmetric stretch of a Q species is its Einstein frequency (ω*). The Einstein frequency is not much different from the Raman shift at 298K [Ω(298)] which may be taken as a reasonable proxy for ω*, as now shown. The Raman frequencies of the symmetric stretch of Q species vary with temperature (Balkanski et al., 1983; Nesbitt et al., 2018) according to:

$$\Omega(T) = \omega^* + C[1 + 2/(e^x - 1)] + D[1 + 3/(e^y - 1) + 3/(e^y - 1)^2] \quad (2)$$

where $\Omega(T)$ is the Raman shift (cm^{-1}) at temperature T (K), ω* is the Einstein frequency, C and

D are constants, $x = h\omega^*/2kT$, $y = h\omega^*/3kT$, h is Planck's constant, k is the Boltzmann constant, and $h\omega^*/k$ is the Einstein temperature (θ_E) of the Raman oscillator. Expansion of Eq. 1 yields:

$$\Omega(T) = \omega^* + C + D + C[2/(e^x - 1)] + D[3/(e^y - 1) + 3/(e^y - 1)^2] \quad (3)$$

Substitution of T = 0 (absolute zero of temperature) into Eq. 2 yields

$$\Omega(0) = \omega^* + C + D \quad (4)$$

and where T = 298 K:

$$\Omega(298) = \Omega(0) + C[2/(e^x - 1)] + D[3/(e^y - 1) + 3/(e^y - 1)^2] \quad (5)$$

Values of $\Omega(T)$ for six Q^2 crystals are plotted on Fig. 1 and the trends were fit using Eq. 2 (Nesbitt et al. 2018). Raman shifts for enstatite and wollastonite were extracted from figures (Zucker and Shim, 2009; Swamy et al., 1997). They are consequently less accurate than the other values and only the ω^* and $C[2/(e^x - 1)]$ terms of Eq. 2 were used for the fit (i.e., D of Eq. 2 = 0.0). The resulting values for $\Omega(298)$, $\Omega(0)$, ω^*, C and D are listed in Table 1 (see caption to Fig. 1 for uncertainties). The C and D coefficients are small so that $\Omega(298)$ and the Einstein frequency (ω^*) differ little at 298K. The $\Omega(298)$ values are used as proxies for ω^* because of their ready availability.

Molecular and average (bulk) polarizabilities

Cationic polarizability has broad application to glasses including aspects related to optical basicity, bond strengths and 'average' electronegativities (Huheey et al., 1997; Reddy et al., 2001; Dimitrov and Komatsu, 2012 and references therein). Cationic polarizabilities reported by Dimitrov and Komatsu (2012), correlate poorly with Q^2 Raman shifts listed in Table 2 (correlation coefficient of 0.42) and although very useful in other regards they are not useful here.

EXPERIMENTAL DATA and CALCULATIONS

Raman shifts for Q^2 species

Raman shifts for the Q^2 symmetric stretch of alkali- and alkaline earth-bearing crystals and glasses at ambient temperatures are listed in Tables 1 and 2. As previously explained, the data selected are, where possible, those for which the temperature dependence of Q^2 Raman shifts are known. There may be variation in Q^2 Raman shifts due to differences in long range order and in site symmetry. Effects of long range order are evident by comparing Ω(298) of wollastonite (composed of Q^2 chains) with Ω(298) of pseudowollastonite (composed of three-membered Q^2 rings). Their Q^2 frequencies differ by ~10 cm^{-1} and Ω(0) by ~15 cm^{-1} at 298 K (Table 1).. The Q^2 frequencies of enstatite and clinoenstatite are split by up to ~ 20 cm^{-1} due to site symmetric effects (e.g., Zucker and Shim, 2009; Chopelas, 1999). Where splitting occurs, average values of the frequencies have been adopted (Table 1).

It has not been possible in some cases to make glasses with 50 mol% M_2O or MO (metasilicate composition) so that Q^2 frequencies were taken from glass spectra containing 30-45mol% modifier oxide *where the Q^2 band was well-resolved*. The Q^2 Raman spectral bands for Na_2SiO_3 and K_2SiO_3 reported by Brawer and White (1975, their Fig. 1) are strongly asymmetric for unknown reasons and are not utilized. Frequencies from better resolved spectra of glasses with 30-40 mol% Na_2O and K_2O are listed in Table 2 (e.g., Frantz and Mysen, 1995, their Fig.9). The shifts are in reasonable agreement. Average values of Ω(298) are listed in Table 2 (third column from the right) and Pauling electronegativities of the counter metal (Huheey et al. 1997) are listed in Tables 1 (last column) and 2 (second last column). The Ω(298) values quoted for individual Q^2 peaks of crystals have uncertainties in measurements of ~2 cm^{-1} whereas those of

glasses typically have uncertainties of ~5-7 cm^{-1} depending on how the spectra were fit. Refer to the original literature sources given in the Tables to evaluate uncertainties of individual bands.

Calculations on $M_6Si_2O_7$ species

Relationships among electronegativities, Raman shifts, and charge distribution on atoms of tetrahedra are explored theoretically using DFT calculations on charge-neutral eclipsed and staggered $M_6Si_2O_7$ (M= Li, Na, K) species (Fig. 2). Following de Jong and Brown (1980) and Uchino et al. (1991; 1992), the dimer was chosen rather than the more complex M_2SiO_3 species to simplify the calculations while retaining the same moieties (e.g., Si-NBO-M, Si-O-Si). To further simplify the calculations, D_{2h} (eclipsed) and D_{3d} (staggered) point-group symmetries were imposed. These restrict the Si-O-Si bond angle to 180°. Each M atom is bidentate (bonded to two NBO atoms) as an attempt to mimic bonding of M atoms in crystals, glasses and melts where they are encased in (and constrained by) oxygen polyhedra. During the vibrational breathing mode, the Si-BO bonds move in and out synchronously, while the Si-NBO bonds move out and in synchronously. GAUSSIAN 03W, Version 6.1 (Frisch et al., 2004) and the DFT method was used for the calculations with the 6-31G+(d):B3LYP basis set:functional combination. Additional details are provided in the Appendix.

RESULTS and INTERPRETATION

Q^2 Raman shifts and Electronegativity

Symmetric stretch frequencies (Tables 1, 2) of Q^2 species in crystals and glasses extend over a range of ~90 cm^{-1} (Figs. 3a, 3b), and the Raman shifts correlate remarkably well with modifier metal electronegativities for both crystals and glasses. The similar temperature dependence of the shifts (Fig. 1) indicates that good correlations should exist at high temperature. Linear least squares fits to the data were performed and the slopes of both trends are

similar but glass frequencies are ~20-30 cm^{-1} lower than for the crystals. Diopside and $Ca_{1/2}Mg_{1/2}SiO_3$ glass, although plotted on Fig. 3 as open circles, were not included in the fits because values for the abscissae of the diagrams cannot be rigorously assessed. The R^2 values indicate that 94% of the variations in Ω(298) of crystals, and 99% of the variations in Ω(298) of glasses, are attributable to the differences in electronegativities of the metal of the modifier oxide. There is no discontinuity in trends between alkali and alkaline earths, indicating that separately, charge and mass of the counter cation have no systematic effect on Ω(298). To emphasize this aspect, the frequencies of Li, Na and Sr glasses are almost identical (Fig. 3b), although masses and charges differ.

Electronegativity is a measure of the tendency of an atom *within a molecule* to attract (or retain) electrons (Pauling, 1960) and the greater the electronegativity of an atom the more likely it will retain its electron density. The converse is also true; the less the electronegativity, the more likely an atom is to transfer electron density to other atoms of a molecule. Of the alkalis and alkaline earths, Mg is most electronegative (Huheey et al., 1997, Table1) and the least electron density should be transferred from Mg to the NBO in glasses or melts. The greatest electron density should be transferred from Cs to NBO. As apparent from the R^2 values (Figs. 2a, 2b), the Q^2 symmetric stretch of crystals and glasses are correlated almost exclusively with the electronegativities of the metals of the modifier oxides.

A common practice is to correlate properties of binary silicate glasses with cation field strength (i.e., $[z^+z^-]/r^2$ where z = nominal charge and r is the cationic radius. There is a strong correlation between electronegativity values and the field strength values of the alkalis and alkaline earths ($R^2 = 0.90$), so that a good correlation must exist between Ω(298) and $(z^+z^-)/r^2$. The relationship for glasses is illustrated in Fig. 3c where a least squares best fit (dashed line)

yields $R^2 = 0.84$. The better correlation is with electronegativity. The question as to why and how electronegativity affects these frequencies is addressed subsequently.

As already noted differences in long range order and crystal site symmetry may alter Q^2 Raman shifts by up to ~20 cm^{-1}, as evident from the data of Table 1 (e.g., wollastonite and pseudowollastonite or enstatite and diopside). Effects of long range order and splitting due to site symmetry cannot, however, explain the large dispersion of Raman shifts observed Figs. 3a and 3b. As for glasses, the dispersion of the alkaline- and alkaline earth-bearing crystals vary sympathetically with the electronegativities of the modifier oxides.

Differences in Q^2 Raman shifts of crystals and glasses

The Q^2 symmetric stretch frequencies of Q^2 species in alkali and alkaline earth crystals is systematically greater than in the equivalent glasses by ~20-30 cm^{-1} (compare Figs. 3a and 3b). Although there is no experimental evidence to explain the crystal-glass offset, it may relate to the differences in volumes. Knocke et al. (1994) provide molar volumes of glasses/melts and their data were extrapolated to obtain the molar volume of 47.52 cm^3mol^{-1} for a 50 mol% Na_2O glass at 298K. The molar volume of Na_2SiO_3(c) is 46.24 cm^3mol^{-1} (McDonald and Cruickshank, 1967). The glass volume is 2.8% greater than the crystal and the effect of increased volume may be to decrease the frequencies of the symmetric stretch. Glass and melt volumes may, for example, be related to the coordination numbers of counter cations (M). Another, more general explanation relates to differences in site potentials arising from long range forces differing in crystals and glasses. This general explanation of course would give rise to differences in volumes as well as other properties. These aspects remain untested because this is not the focus of the study.

Electronegativity and valence electron densities

The explanation for the trends of Figs. 3a and 3b begins with the effect of alkali and alkaline earths electronegativity on the valence charge density on Si and O atoms of SiO_4 tetrahedra. All Group I and II metals are less electronegative than O and Si and wherever M-O bonds exist, charge will be transferred from M to O atoms, thus increasing electron density on NBO atoms (and BO atoms where M is bonded to a BO). Moreover, the lower the electronegativity of the metal 'M', the *greater will be the* charge transferred and the greater the electron density on the associated NBO. The increased charge density on NBO atoms is redistributed (delocalized) over the other atoms of the tetrahedron via the four equivalent Si sp^3 hybrid molecular orbitals (Pantellides and Harrison, 1976; de Jong and Brown, 1980; Uchino et al. 1992; Demiralp et al., 1999; Nesbitt et al., 2017a,b). As a result, the electronegativity of the metal 'M' affects the electron density on all atoms of SiO_4 tetrahedra.

The explanation of charge-transfer has been simplified by assuming that the metal atom 'M' transfers charge to tetrahedra only through NBO. The argument is too restrictive because M may approach BOs as closely as it does NBOs, as apparent from study of crystalline phases (e.g., Na-silicates, McDonald and Cruickshank, 1967; Ching et al., 1983). Where M-BO and M-NBO are separated by similar distances, charge is likely to be transferred via both NBO and BO to tetrahedra, thus allowing numerous 'pathways' by which charge is lost from M and acquired by Si and O atoms of tetrahedra.

The increased electron density on Si and O atoms has been confirmed by X-ray Photoelectron Spectroscopy (XPS) through measurement of binding energies (BEs) of core and valence orbitals of silicate crystals and glasses (Hsieh et al. 1994; Namba et al. 2003; Nesbitt et al., 2011; 2014; 2017a,b; Sawyer et al., 2012; 2015). The BEs of Si 2p, O 1s of BOs and O 1s of NBOs all decrease with increased Na and K content of the glasses (Fig. 4). The decreases in BEs

(referred to as chemical shifts) result from transfer of outermost 's' electrons of Na and K to NBO and on to Si and BO atoms of the tetrahedron via sp^3 hybrid bonds (Carlson, 1975; Namba et al., 2003; Nesbitt et al. 2017a,b). The charge originating on the metal becomes delocalized over the entire tetrahedron. The chemical shifts are greater for potassic glasses than for sodic glasses, a consequence of K having a lower electronegativity than Na. The relationship between electronegativity and charge density is most apparent for the NBO O1s data of Fig. 4a. The NBO 1s BEs are consistently ~0.5 eV less for potassic glasses than for the sodic glasses, demonstrating that there is greater electron density on the NBO associated with K than with Na. The K and Na electronegativity differences also explain the slopes of the BO 1s and Si 2p trends in that they are steeper for K-silicate glasses than for Na-silicate glasses.

Namba et al. (2003) and Nesbitt et al. (2017a,b) note that increased alkali content causes a greater chemical shift (i.e., ΔBE) for the Si 2p signal than for the O 1s signal of either BO or NBO (as indicated by the slopes of the trends of Figs 4a and 4b). The greater slope of the Si 2p trend (greater ΔBE) indicates preferential accumulation of negative charge on Si relative to BO and NBO atoms. The accumulation of charge on Si (relative to O) is, in fact, greater than the plot indicates because the sensitivity of the Si 2p BE to a unit charge 'q' is about one-half that of O. This arises because ΔBE (i.e., chemical shift), is to a first approximation (Carlson et al. 1975):

$$\Delta BE = \Delta q \, (e^2/\langle r_v \rangle) \qquad (7)$$

where Δq is the change in valence charge on either Si or O, and $e^2/\langle r_v \rangle$ is the reciprocal of the mean radius of the valence orbital being considered (Carlson, 1975, Table 5.7). Expressed in eV, these values are: 31.6 eV for O 2p, 13.8 eV for Si 3p, and 18.1 eV for Si 3s. Using the weighted mean for the Si sp^3 hybrid, one obtains an $e^2/\langle r_v \rangle$ of 14.9 eV, which is close to half of that for O 2p given above. From Eq. 7, and using the above slopes (0.023, 0.037, and 0.054) as measures of

ΔBE, one obtains Δq_{Si} ~5Δq_{BO} and Δq_{Si} ~3q_{NBO}. A Δq of 0.1 results in a ΔBE of ~3eV for O 1s (Eq. 7) and a ΔBE of ~1.5eV for Si 2p. Relaxation and point charge effects decrease ΔBE of both by up to 50% (Carlson, 1975; Hsieh et al. 1994; Nesbitt et al. 2017a,b). The calculations explain the magnitudes of the Si 2p and O 1s chemical shifts and the slopes observed in Fig. 4. They are due to increased charge on both Si and O atoms of tetrahedra, the charge being transferred from K and Na. Proportionally greater charge is transferred from the former metal than the latter, in accordance with their electronegativities. Figure 4 and the calculations also point to the importance of partial charges on Si and O atoms, as discussed in more detail in the section on computations.

Raman shifts and XPS BEs related

Figures 3 and 4 illustrate that both Raman shifts and Si 2p BEs decrease with charge transfer from alkalis and alkaline earths to Si and O atoms of tetrahedra. A direct correlation is therefore expected between Raman shifts and Si 2p BEs for both crystals and glasses. Raman and XPS data for some crystals and glasses listed in Table 3 are plotted on Fig. 5. The solid line indicates the trend for crystals and the dashed line the trend for glasses. For the crystals, both Raman shift and Si 2p BE decrease sympathetically from cristobalite to pyroxenes (en, di) and to forsterite. Similarly for Na glasses (Fig. 5, dashed line), there is a sympathetic decrease in both variables. The trends are confirmation of the relationship among charge transfer, Raman shifts and BEs. To emphasize this aspect consider the two compositionally equivalent metasilicate Q^2 species, Na_2SiO_3 glass and enstatite ($MgSiO_3$). Na is less electronegative than Mg, so that a greater portion of charge ('s' electrons) should be transferred from Na to Q^2 compared with that transferred from Mg to Q^2. The greater charge transfer from Na is confirmed in that the change in Raman shift *and* Si 2p BE are greater for Na_2SiO_3 than for $MgSiO_3$.

The sympathetic relationships between Raman shifts and Si 2p chemical shifts (Fig. 5) are simply explained if *both* are controlled by the electron density on Q species. This argument also explains the dispersion of Raman shifts observed for crystals and glasses of Fig. 3; the dispersion results from variable of electron densities on Si and O atoms of Q^2 tetrahedra with the electron densities being controlled by the electronegativities of Groups 1 and 2 metals. Preferential accumulation of electronic charge on Si (Fig. 4) relative to O weakens all Si-O coulombic interactions and Si-BO and Si-NBO force constants. Decreased force constants are manifested in the SiO_4 symmetric stretch frequencies, which decrease according to Eq. 1 and as shown in Fig. 3. Apparently the partial charges on Si and O atoms of tetrahedra are a critically important control on the frequencies of the symmetric stretch of Q species.

COMPUTATIONS

The data of Table 4 lists properties derived from the calculations on the six model $M_6Si_2O_7$ structures (Fig. 2) where M= Li, Na, K and where Si-O-Si bond angles are fixed at 180 degrees. Although there are similar calculations on $M_xH_{4-x}Si_2O_7$ molecules with M = Li, Na and K (de Jong and Brown, 1980; Uchino et al.1991, 1992), this is the first to use only alkali cations bonded to NBOs (i.e., no H) and to report reduced masses, force constants and Raman shifts. Brown et al. (1969) demonstrated that Si-O bond lengths in framework silicates varied depending on the Si-O-Si angle. The angle was held constant in these calculations. this has the advantage of emphasizing the effects of other aspects such as charge distribution among atoms of the tetrahedra and the modifier cations.

Reduced masses

The reduced masses in Table 4 range from 18.8 to 20.2 and average 19.5 mass units. Are these reasonable? The $M_6Si_2O_7$ molecule consists of two SiO_4 tetrahedra of staggered and

eclipsed geometries, sharing a BO atom (Fig. 2). The two Si atoms of the staggered form move synchronously toward and away from the BO atom, which is stationary. The reduced mass includes the Si atom (=28.1 mass units). With O of 16 mass units, and BO stationary, total mass of the O atoms is 3x16 mass units and the reduced mass is:

$$\mu = \{(28.1\bullet(3\bullet16))/(28.1+(3\bullet16))\} = 17.7 \text{ mass units}$$

The calculation assumes that the six M cations have no effect on the reduced mass. Inclusion of BO in the calculation increases the reduced mass to 19.5 which is similar to those reported in Table 4. Apparently, other contributions to 'μ' such as the alkalis, are minor, a finding consistent with the calculations of (Furukawa et al., 1981).

Raman shifts and force constants

The simulated frequencies of the symmetric stretch for $Li_2Si_2O_7$, $Na_2Si_2O_7$ and $K_2Si_2O_7$ average, respectively, 902 cm^{-1}, 856 cm^{-1} and 831 cm^{-1}. The review by McMillan (1984) reports an average value of ~900 cm^{-1} and our values compare well with the 889 cm^{-1} value calculated by Furukawa et al. (1981) for the Si_2O_7 dimer (their Table II). The systematic decrease in frequencies from ~902 cm^{-1} to ~831 cm^{-1} cannot be ascribed to the masses of the alkalis. It is, instead, related to the electronegativities of the alkalis and to transfer of charge to NBO and on to Si and O atoms of tetrahedra thus changing the electron densities on these atoms. K is the least electronegative, thus it transfers the greatest portion of charge to NBO and Li transfers the least charge. The redistribution of charge throughout the tetrahedron and its preferential accumulation on Si weakens the coulombic Si-O interaction and the associated force constant thus decreasing the frequency of the symmetric stretch (Table 4). Although the masses of the alkali cations do not affect the symmetric stretch, their electronegativities do, and the variations in the latter property explain the trends of Fig. 3.

The force constants derived from the calculation (Table 4) range from 7.5×10^5 to 9.7×10^5 dynes/cm. The values selected by Furukawa et al. (1981) were somewhat less, at 5×10^5 (Si-BO) and 4.5×10^5 (Si-NBO) dynes/cm. The force constants derived for some crystals, however, range from 10.0×10^5 to 8.3×10^5 dynes/cm (e.g., Fleet and Henderson, 1997; McKeown et al., 1996; Le Cleac'h and Gillet, 1990). The force constants obtained from the calculations seem reasonable. Most importantly, their values are dependent on the electronegativities of the alkali bonded to NBO. These calculations corroborate our earlier conclusion that the force constants and the frequencies of vibration are determined primarily by the partial charges on the atoms of the tetrahedron.

Bond lengths and bond angles

The simulated Si-BO bond lengths of the $M_6Si_2O_7$ molecules vary from 1.63Å to 1.65Å to 1.67Å in the order Li<Na<K. These conform to bond lengths observed for crystalline and glassy silicates (Shannon, 1976; Liebau, 1985, Chap. 3). The simulated Si-NBO bond lengths (Table 4) are all 1.66Å and independent both of the nature of the cation and of the form of the molecules. The Si-NBO bond lengths are, however, slightly greater than Si-BO bond lengths for the Li and Na forms (Table 4) and consequently contravene the general relationship where Si-BO distances are slightly greater than Si-NBO bond lengths in silicate glasses (Liebau, 1985, Chap 3). This may result from constraining the Si-O-Si bond angle to 180° (Brown et al., 1969) and from NBO-M bonding, where the M atoms are bonded to two NBO atoms only. They are typically bonded to more O atoms in glasses, thus there likely is freer, and more extensive vibrational motion in the calculations than is realistic. The M-O bond lengths derived from the calculations (Table 4) are 0.1- 0.2Å shorter than values obtained by summing ionic radii of Shannon (1976) but are similar to literature crystalline and glass values (e.g., Gagné and

Hawthorne, 2016; Smyth and Hazen, 1973; McDonald and Cruikshank, 1967; Ghose et al. 1986). The M-O, Si-NBO and Si-BO bond lengths are not correlated with electronegativities of the cations in these calculations. Neither do simulated and measured bond lengths correlate strongly with Si-O force constants, or with symmetric stretch frequencies. Apparently, there is no systematic relationship between force constants and bond lengths in silicates.

Calculations on Na silicate crystals and glasses yield Si-O bond lengths of about 1.6 Å (e.g., Cormack et al., 2002; 2003; Du and Corrales, 2006; Yamamoto et al., 2017), but these papers have emphasized that both ab-initio and MD calculations may not represent accurately interatomic potentials (IP) and force fields especially for glasses. Yamamoto et al. (2017), for example, used two IP's on a range of compositions from SiO_2 to Na_2SiO_3 where partial charges on Si and O atoms were allowed to vary with composition. They obtained constant Si-O bond lengths of 1.64Å (IP1) and 1.57Å (IP2) regardless of glass composition even though Si and O partial charges changed with composition. Clearly, aspects other than charge affect bond lengths in these calculations, although they were not elucidated. MD calculations on Li, Na, K silicate glasses by Du and Corrales (2006) used the same charges on the Si (+2.4), O (-1.2), and Li, Na, K (+0.6) for all glasses containing up 50 mol% M_2O. The simplification is unrealistic and in conflict with the experimental XPS results.

In our calculations (Table 4) all cations are bonded to two NBOs and this bidentate bonding yields systematic change in M-NBO-M bond angles with the increasing size of the cation (Table 4). The average O-Si-O bond angle is ~109° in all six structures and, as for bond lengths, this angle does not correlate with electronegativity of the modifier oxides or their size. Both BO-Si-NBO and NBO-Si-NBO angles correlate with the size of the cation but in opposite senses. The O-M-O and M-O-M angles correlate very strongly with cation size but again in

opposite senses.

Mulliken, AIM and partial charges from XPS

Mulliken and AIM (atoms-in-molecules) charges on Si, NBO, BO and M of the $M_6Si_2O_7$ molecules are listed in Table 4. The Mulliken partial charges on Li, Na and K average +0.44, +0.84 and +0.86 for both staggered and eclipsed forms, hence Li loses least and K loses most charge, as expected from their electronegativities. Other studies yield similar values. Yamamoto et al. (2017) obtained partial charges on Na of +0.9(±0.1) for glasses containing 30-67 mol% Na_2O and Uchino et al. (1991) and de Jong and Brown (1980) obtained respectively +0.7±0.05 and 0.75 on Na of simulated $H_5Na_1Si_2O_7$, $H_4Na_2Si_2O_7$ and $H_2Na_4Si_2O_7$ molecules. Uchino et al. (1992) modelled $H_5Li_1Si_2O_7$, $H_5Na_1Si_2O_7$ and $H_5K_1Si_2O_7$ molecules yielding partial charges for Li, Na, and K respectively of ~0.60, ~0.70 and ~0.81 whereas and de Jong and Brown (1980) obtained respectively, ~0.49, ~0.75 and ~0.89. The calculations yield Mulliken partial charges on Na intermediate between the partial charges on Li and K as expected from electronegativities. Note, however, the comparatively high charge on Na obtained by our calculations. The calculations of de Jong and Brown (1980), Uchino et al. (1991; 1992), Namba et al. (2003) for $Na_2Si_2O_5$ and Na_2SiO_3 crystals, and Hsieh et al. (1994) for $Na_2Si_3O_7$ glass obtained partial charges on Na between ~0.8 and ~0.6. Our values (Table 4) seem somewhat too positive.

The Mulliken Si charges from our calculations range from +1.14 to +1.72 (Table 4). Other calculations have obtained Si charges ranging between +2.3 and +1.27 on vitreous and crystalline SiO_2, Na silicates and model compounds (Yamamoto et al., 2017; Hsieh et al., 1994; Demiralp et al., 1999; Uchino et al., 1992; de Jong and Brown, 1980). The range of the Si charges is reasonable. Our calculations do not, however, demonstrate a systematic change in Si charge as a function of metal electronegativity. The Si charge on $Na_6Si_2O_7$ is, for example

greater than on $K_6Si_2O_7$ which is opposite to that expected from the electronegativities of the metals (Table 4). Similarly, $Na_6Si_2O_7$ displays aberrant NBO and BO charges with respect to those of $Li_6Si_2O_7$ and $K_6Si_2O_7$. The lack of regular trends in the charges on Si, NBO and BO (Table 4) is not readily explained other than to conclude that calculated and XPS results are not consistent. To emphasize the difficulties in calculating these charges, Uchino et al. (1992) used ab initio calculations to obtain Mulliken charges in the model cluster $Na_2H_4Si_2O_7$. Using four different basis sets, they obtained Si charges ranging between +1.462 and +1.937. Additional studies are required to reconcile XPS experiment results with calculations.

Namba et al. (2003) used DV-Xα cluster MO calculations and population analysis to obtain Mulliken charges on Si for vitreous and crystalline SiO_2, for $Na_2Si_2O_5$ glass in which Q^3 species dominates, and for Na_2SiO_3 glass in which Q^2 species dominates. Plotted at the top of Fig. 5 are the Si charges calculated by Namba et al. (2003). Their results enable evaluation of the partial charge on Si for the metasilicate crystals, enstatite ($MgSiO_3$) and diopside ($Ca_{0.5}Mg_{0.5}SiO_3$) by interpolating between the Si charge on SiO_2 (~2.1) and on the disilicate glasses (~1.95). A Si charge of ~2.0 is obtained. The Si charge of ~2.0 applies to Si of the Q^2 species of these crystals. The Na_2SiO_3 glass also consists predominantly of Q^2 species but the Si charge of this phase is ~1.8, which differs from that on enstatite by ~0.2. The difference in charge on Si of ~0.2eV (between $MgSiO_3$ and Na_2SiO_3) is largely responsible for the difference in the Raman shift of two phases, which is ~70 cm^{-1} (Fig. 5, Table 3). The more positive charge on Si of enstatite results in a weaker Si-O Coulombic attraction (weaker bond) and a decreased frequency for the Q^2 symmetric stretch. This is a first attempt to relate Si charges to Raman shifts. High quality ab initio calculations of the Q^2 Raman shift for crystalline metasilicates are required where the effects of different counter cations are *compared and contrasted*. Belmonte et

al. (2016), for example, obtained a Raman shift of 955 cm^{-1} for Na_2SiO_3 whereas the experimental shift is 966 cm^{-1} (Richet et al. 1996).

The calculated AIM charges on the metal atoms of the three $M_6Si_2O_7$ molecules differ minimally, ranging between +0.91 and +0.87 (Table 4). The positive charges on the M atoms are in the order Li>Na>K (i.e., 0.91, 0.89 and 0.87) and contrary to that expected from electronegativities and XPS results. AIM charges and their meaning require additional study as has also been suggested previously (Dean, 2018).

IMPLICATIONS

An important question is raised by these observations. How can the Raman shifts and the XPS BE changes be so pronounced without Si-O bond lengths changing appreciably? As previously noted, Si-O bond lengths are similar (within 0.02Å) for widely varying orthosilicate and metasilicate compositions. In diatomic molecules, force constants and bond lengths are directly related (e.g., Smith, 1968 and references therein). In great contrast, bond lengths are not directly related to force constants and Raman shifts in these silicate condensed phases! Pantelides and Harrison (1976), for example, show a large range of Si-O bond lengths for different SiO_2 polymorphs where Si-O bond lengths vary from 1.55Å in β-cristobalite to 1.63Å in β-quartz. In addition, Demiralp et al. (1999) showed that Si charges vary from +1.216 in β-cristobalite to +1.32 in α-quartz and vitreous SiO_2. Perhaps Si-O bond lengths are more sensitive to crystal packing forces than to Si-O force constants.

The above observations indicate that several factors should be considered where testing ab-initio or MD calculations. First, reproduction of Si-O bond lengths is a necessary test, but not a sensitive test of the veracity of a calculation. Reproduction of Raman shifts would seem to be a much more sensitive test. Also, and perhaps most importantly, no study has conducted a

comprehensive, comparative analysis of charge redistribution on M, Si or O atoms of binary silicate glasses (or melts) containing different modifier oxides. Included in such a study should be an attempt to evaluate the effects of partial charges on Raman shifts.

Theoretical calculations seem to be the best avenue to reconcile these aspects. Ab-initio calculations should be the best approach but they commonly are not practical for many large systems such as silicate glasses where long times are required for proper calculation (e.g., Liu et al., 1994; Stixrude and Karki, 2005; de Koker et al., 2009; Spiekermann et al., 2013; Belmonte et al., 2016). Classical molecular dynamics (MD) calculations typically prescribe force fields and potential energy characteristics in place of (or in conjunction with) ab-initio calculations. Both approaches have shortcomings in that force fields calculated from first principles or prescribed (MD calculations) may not be accurate representations of actual fields and potentials in the condensed phases considered here (e.g., Cormack et al., 2002; 2003; Mantisi and Micoulaut, 2016; Yamamoto et al., 2017). Perhaps the most striking of these problems is highlighted by recent calculations by Yamamoto et al. (2017) on Na silicate glasses. They used two potentials which yielded different Si-O bond lengths for the same glasses, 1.57Å and 1.64Å. These did not vary with glass composition, which is in stark contrast to the EXAFS/XANES studies of Henderson (1995) and McHale et al. (1988) where bond lengths varied with composition (from 1.59Å to 1.67Å). Secondly, Yamamoto et al. (2017) evaluated the coefficient of thermal expansion (α) using the two potentials and both yielded underestimates. Tomlinson et al. (1958) noted that 'α' was dependent on coulombic attractive forces between M and O but the potentials used do not seem to have captured accurately these interactions. Third, Yamamoto et al. (2017) do not distinguish between NBO and BO, but Na interacts more with NBO than BO as noted by Cormack et al. (2002; 2003). Nevertheless, their effort to address partial charges is commended

and similar efforts are required of future ab-initio and MD calculations because charges affect dramatically Si-O force constants and associated vibrational frequencies as illustrated in Fig. 3.

In addition, calculations should be tested against Raman and XPS experimental results. This may be done by comparing calculated and experimental changes to charge density on atoms of crystals and glasses as a function of modifier oxide type, and as a function of modifier oxide content (e.g., Fig. 4). Demiralp et al. (1999) used the charge equilibration procedure of Rappé and Goddard (1991) which allowed charges to be adjusted as geometric configurations changed for SiO_2 crystals and glass. Additional insight and modelling are required to fully understand and explain the partial charges on Si, BO and NBO, and an appreciation of electronegativities should be an important aid to interpretation of results.

CONCLUSIONS

The range of Raman shifts (over ~90 cm^{-1}), Si 2p and O 1s XPS BEs (over 2 eV) observed for Q^2 species of alkali silicate glasses and crystals results ultimately from the differences in modifier cation electronegativities. The largest Raman shift and the largest XPS BEs chemical shifts are observed for the most electronegative cation, Mg. The electronegativity of the metal controls the extent to which 's' electrons are donated to NBO and delocalized over all atoms of SiO_4 tetrahedra. As noted by several XPS studies (Namba et al. 2003; Hsieh et al.1994; Nesbitt et al. 2017a,b), the electron density on Si increases more than the charge on the O atoms of tetrahedra resulting in a weakened Coulombic interaction between the two, thus weakening Si-O bonds, which results in the decrease in the symmetric stretch frequencies of Q^2 species. Ab-initio calculations on $M_6Si_2O_7$ (M=Li,Na,K) species corroborate the important effect of electronegativity on Raman shifts.

ACKNOWLEDGEMENTS

The authors thank their respective Universities and departments for the logistical and financial support required to conduct this study. PAWD thanks Dr. G.D. Willett of the School of Chemistry, UNSW, for the use of his GAUSSIAN and GAUSSVIEW programs.

References

Balkanski, M., Wallis, R.F., and Haro, T. (1983) Anharmonic effects in light scattering due to optical phonons in silicon. Physical Review, 28, 1928–1934.

Bader, R.F.W. (2005) Quantum Mechanical Basis for Conceptual Chemistry. Monatshefte für Chemie, 136, 819-854.

Bancroft, G.M., Nesbitt, H.W., Henderson, G.S., O'Shaughnessy, C., Withers, A.C., and Neuville, D.R. (2018) Lorentzian dominated lineshapes and linewidths for Raman symmetric stretch peaks (800–1200 cm−1) in Q^n (n=1–3) species of alkali silicate glasses/melts. Journal of Non-Crystalline Solids, 484, 72-83.

Belmonté, D., Gatti, C., Ottonello, G., Richet, P., and Zuccolini, M.V. (2016) Ab Initio thermodynamic and thermophysical properties of sodium metasilicate, Na_2SiO_3, and their electron-density and electron-pair-density counterparts. Journal of Physical Chemistry A, 120, 8881-8895.

Brawer, S.A., and White, W.B. (1975) Raman spectroscopic investigation of the structure of silicate glasses. I. The binary alkali silicates. Journal of Chemical Physics, 63, 2421-2432.

Brown, G.E., Gibbs, G.V., and Ribbe, P.H. (1969) The nature and the variation in length of the Si-O and Al-O bonds in framework silicates. American Mineralogist, 54, 1044-1061.

Carlson, T.A. (1975) Photoelectron and Auger Spectroscopy. Plenum Press, New York, 417p.

Ching, W.Y., Murray, R.A., Lam, D.J., and Veal, B.W. (1983) Comparative studies of electronic structures of sodium metasilicate and a and {3 phases of sodium disilicate. Physical

Review B, 28, 4724-4735.

Chopelas, A. (1991) Single crystal Raman spectra of forsterite, fayalite, and monticellite. American Mineralogist 76, 1101-1109.

Chopelas, A. (1999) Estimates of mantle relevant Clapeyron slopes in the $MgSiO_3$ system from high-pressure spectroscopic data. American Mineralogist, 84, 233-244.

Choudhury, N., Ghose, S., Chowdhury, C.P., Loong, C.K., and Chaplot, S.L. (1998) Lattice dynamics, Raman spectroscopy, and inelastic neutron scattering of orthoenstatite $Mg_2Si_2O_6$. Physical Review B, 58, 756-765.

Cormack, A.N., Du, J., and Zeitler, T.R. (2002) Alkali ion migration mechanisms in silicate glasses probed by molecular dynamics calculations. Physical Chemistry Chemical Physics, 4, 3193–3197.

Cormack, A.N., Du, J., and Zeitler, T.R. (2003) Sodium ion migration mechanisms in silicate glasses probed by molecular dynamics calculations. Journal of Non-Crystalline Solids, 323, 147-154.

Dean, P.A.W. (2018) The not-so-simple coordination chemistry of alkali-metal cations Li^+, Na^+ and K^+ with one carbonate anion: A study using density functional and atoms in molecules theories. Inorganica Chimica Acta, 469, 245-254.

de Jong, B.H.W.S., and Brown, G.E. (1980) Polymerization of silicate and aluminate tetrahedra in glasses, melts and aqueous solutions- II. The network modifying effects of Mg^{2+}, K^+, Na^+, Li^+, H^+, OH^-, F^-, Cl^-, H_2O, CO_2 and H_3O^+ on silicate polymers. Geochimica et Cosmochimica Acta, 44, 1627-1642.

de Koker, N.P., Stixrude, L., and Karki, B.B., (2009) Thermodynamics, structure, dynamics, and freezing of Mg_2SiO_4 liquid at high pressure. Geochimica et Cosmochimica Acta, 72,

1427–1441.

Demiralp, E., Cagin, T., and Goddard III, W.A. (1999) Morse stretch potential charge equilibrium force field for ceramics: application to the quartz-stishovite phase. Physical Review Letters, 82, 1708–1711.

Dennington, II, R., Keith, T., Millam, J., Eppinnett, K., Hovell, W.L., and Gilliland, R. (2003) Gaussview 4.1, Semichem, Inc., Shawnee Mission, KS.

Dimitrov, V., and Komatsu, T. (2012) Correlation among electronegativity, cation polarizability, optical basicity and single bond strength of simple oxides. J. Solid State Chem. 196, 574-578.

Du, J., and Corrales, L.R. (2006) Compositional dependence of the first sharp diffraction peaks in alkali silicate glasses: A molecular dynamics study. Journal of Non-Crystalline Solids, 352, 3255-3269.

Fleet, M.E., and Henderson, G.S. (1997) Structure-composition relations and Raman spectroscopy of high-pressure sodium silicates. Physics and Chemistry of Minerals, 24, 345–355.

Frantz, J.D., and Mysen, B.O. (1995) Raman spectra and structure of $BaO-SiO_2$, $SrO-SiO_2$ and $CaO-SiO_2$ melts to 1600°C. Chemical Geology, 121, 155-176.

M.J. Frisch, G.W. Trucks, H.B. Schlegel, G.E. Scuseria, M.A. Robb, J.R. Cheeseman, J.A. Montgomery Jr., T. Vreven, K.N. Kudin, J.C. Burant, J.M. Millam, S.S. Iyengar, J. Tomasi, V. Barone, B. Mennucci, M. Cossi, G. Scalmani, N. Rega, G.A. Petersson, H. Nakatsuji, M. Hada, M. Ehara, K. Toyota, R. Fukuda, J. Hasegawa, M. Ishida, T. Nakajima, Y. Honda, O. Kitao, H. Nakai, M. Klene, X. Li, J.E. Knox, H.P. Hratchian, J.B. Cross, V. Bakken, C. Adamo, J. Jaramillo, R. Gomperts, R.E. Stratmann, O. Yazyev,

A.J. Austin, R. Cammi, C. Pomelli, J.W. Ochterski, P.Y. Ayala, K. Morokuma, G.A. Voth, P. Salvador, J.J. Dannenberg, V.G. Rabuck, K. Raghavachari, J.B. Foresman, J.V. Ortiz, Q. Cui, A.G. Baboul, S. Clifford, J. Cioslowski, B.B. Stefanov, G. Liu, A. Liashenko, P. Piskorz, I. Komaromi, R.L. Martin, D.J. Fox, T. Keith, M.A. Al-Laham, C.Y. Peng, A. Nanayakkara, M. Challacombe, P.M.W. Gill, B. Johnson, W. Chen, M.W. Wong, C. Gonzalez, J.A. Pople, (2004) GAUSSIAN 03, Revision D.01, GAUSSIAN Inc, Wallingford, CT.

Furukawa, T., Fox, K., and White, W.B. (1981) Raman spectroscopic investigation of the structure of silicate glasses. III. Raman intensities and structural units in sodium silicate glasses. Journal of Chemical Physics, 75, 3226-3237.

Gagné, O.C., and Hawthorne, F.C. (2016) Bond-length distributions for ions bonded to oxygen: alkali and alkaline-earth metals. Acta Crystallographica, B72, 602-625.

Ghose,S., Schomaker,V., and McMullan, R.K. (1986) Enstatite, $Mg_2Si_2O_6$: A neutron diffraction refinement of the crystal structure and a rigid-body analysis of the thermal vibration. Zeitschrift für Kristallographie, 176, 159-175.

Henderson, G.S. (1995) A Si K-edge EXAFS/XANES study of sodium silicate glasses. Journal of Non-Crystalline Solids, 183, 43-50.

Hsieh, C.H., Jain, H., Miller, A.C., and Kamitsos, E.I. (1994) X-ray photoelectron spectroscopy of Al- and B-substituted sodium trisilicate glasses. Journal of Non-Crystalline Solids, 168, 247-257.

Huheey, J.E., Keiter, E.A., and Keiter, R.L. (1997) Inorganic Chemistry: Principles of Structrure and Reactivity (4th ed.). Pearson, 964 p.

Kalampounias, A.G., Nasikas, N.K., and Papatheodorou, G.N. (2009) Glass formation and

structure in the $MgSiO_3$-Mg_2SiO_4 pseudobinary system: From degraded networks to ionic like glasses. Journal of Chemical Physics, 131, 114513 (1-8).

Keith, T. A. (2017), AIMAll, Professional. TK Gristmill software, Overland Park, KS, USA. (aim.tkgristmill.com)

Knocke, R., Dingwell, D.B., Seifert, F.A., and Webb, S.L. (1994) Non-linear properties of supercooled liquids in the system Na_2O-SiO_2. Chemical Geology, 116, 1-16.

Le Cléac'h, A., and Gillet, P. (1990) IR and Raman spectroscopic study of natural lawsonite. European Journal of Mineralogy, 2, 43-52.

Liebau, F. (1985) Structural Chemistry of Silicates. Springer-Verlag, Berlin, 354p.

Liu, F., Garofalini, S. H., Kingsmith, D. and Vanderbilt, D. (1994) First-principles study of crystalline silica. Physical Review B, 49, 12528-12534.

Mantisi, B., and Micoulaut, M. (2016) Premelting and cation mobility in simple silicates: contrasting dynamics in the crystalline and molten state. Journal of Non-Crystalline Solids, 2016, 440, 1−6.

Matson, D.W., Sharma, S.K, and Philpotts, J.A. (1983) The structure of high-silica alkali-silicate glasses. A Raman spectroscopic investigation. Journal of Non-Crystalline Solids, 58, 323-352.

McDonald, W.S., and Cruickshank D.W.J. (1967) A Reinvestigation of the Structure of Sodium Metasilicate, Na_2SiO_3. Acta Crystallographica, 22, 37-43.

McHale, A.G., Veal, B.W., Paulikas, A.P., Chan, S.K., and Knapp, G.S. (1988) Improved ab Initio Calculations of Amplitude and Phase Functions for Extended X-ray Absorption Fine Structure Spectroscopy. Journal of the American Chemical Society, 110, 3763-3768.

McKeowen, D.A., Nobles, A.C., and Bell, M.I. (1996) Vibrational analysis of wadeite

$K_2ZrSi_3O_9$ and comparisons with benitoite $BaTiSi_3O_9$. Physical Review B, 54, 291-304

McMillan, P.F. (1984). Structural studies of silicate glasses and melts – applications and limitations of Raman spectroscopy. American Mineralogist, 69, 622-644.

Moelwyn-Hughes, E.A. (1964) Physical Chemistry. 2nd ed., Franklin Book Co; 1333 p.

Moulton, B.J., Gomes, E.O., Cunha, T.R., Doerenkamp, C., Gracia, L., Eckert, H., Andrés, J. Pizani, P.S. (2021) A Theoreticcal and experimental investigation of hetero- versus homo-connectivity in barium silicates. American Mineralogist, preprint, DOI https//doi.org/10.2138/am-2021-7910.

Mulliken, R.S. (1955) Electronic population analysis on LCAO-MO molecular wave functions. Journal of Chemical Physics, 23, 1833-1849.

Mysen, B.O., Virgo, D., and Seifert, F.A. (1982) The structure of silicate melts: Implications for chemical and physical properties of natural magma. Reviews in Geophysics and Space Science, 20, 353-383.

Mysen, B.O., and Frantz, J.D. (1992) Raman spectroscopy of silicate melts at magmatic temperatures: Na_2O-SiO_2, K_2O-SiO_2 and Li_2O-SiO_2 binary compositions in the temperature range 25-1475°C. Chemical Geology, 96, 321-332.

Mysen, B.O., and Frantz, J.D., (1993) Structure and properties of alkali silicate melts at magmatic temperatures. European Journal of Mineralogy, 5, 393-407.

Namba, T., Hagiwara, T., and Miura, Y. (2003) Chemical bonding state of sodium silicates. Advances in Quantum Chemistry, 42, 187-198.

Nasikas, N.K, Chrissanthopoulos, A., Bouropoulos, N., Sen, S., and Papatheodorou, G.N. (2011) Silicate Glasses at the Ionic Limit: Alkaline-Earth Sub-Orthosilicates. Chemical Materials, 23, 3692-3697.

Nesbitt H.W., and Bancroft G.M., (2014) High resolution core- and valence-level XPS studies of the properties (structural, chemical and bonding) of silicate minerals and glasses. Advances in Raman Spectroscopy Applied to Earth and Material Sciences. Reviews in Mineralogy and Geochemistry, 78, 271-329.

Nesbitt H.W., Bancroft G.M., Henderson G.S., Ho R., Dalby K.N., Huang Y., and Yan Z., (2011) Bridging, non-bridging and free (O^{2-}) oxygen in Na_2O-SiO_2 glasses: An x-ray photoelectron spectroscopic (XPS) and nuclear magnetic resonance (NMR) study. Journal of Non-Crystalline Solids, 357,170-180.

Nesbitt, H.W., Henderson, G.S., Bancroft, G.M., and O'Shaughnessy, C. (2017a) Electron densities over Si and O atoms of tetrahedra and their impact on Raman stretching frequencies and Si-NBO force constants. Chemical Geology, 461, 65-74.

Nesbitt, H.W., Bancroft, G.M., and Ho, R, (2017b) XPS valence band study of Na-silicate glasses: energetics and reactivity. Surface and Interface Analysis, 49, 1298–1308.

Nesbitt H.W., Bancroft, G.M., and Henderson, G.S. (2018) Temperature dependence of Raman shifts and line widths for Q^0 and Q^2 crystals of silicates, phosphates, and sulfates. American Mineralogist, 103, 966-976.

Nesbitt, H.W., Henderson, G.S., and Bancroft, G.M., (2019) Factors affecting line shapes and intensities of Q^3 and Q^4 Raman bands of Cs silicate glasses. Chemical Geology, 505, 1-11.

Nesbitt, H.W., Bancroft, G.M., and Henderson, G.S. (2021) Nucleophilic substitution reaction mechanisms: An atomic-molecular perspective on chemical speciation and transport properties in silicate melts. Chemical Geology, 555, 119818-1—119818-12.

Neuville, D.R. (2006) Viscosity, structure and mixing in (Ca, Na) silicate melts. Chemical

Geology, 229, 28-41.

O'Shaughnessy C., Henderson G.S., Nesbitt H.W., Bancroft G.M., and Neuville D.R. (2020) The influence of modifier cations on the Raman stretching modes of Q^n species in alkali silicate glasses. Journal of the American Ceramic Society, 103, 3991–4001.

Pantelides, S.T., and Harrison, W.A. (1976) Electronic structure, spectra, and properties of 4:2coordinated materials: Crystalline and amorphous SiO_2 and GeO_2. Physical Review B, 13, 2667-2674.

Pauling, L. (1960) The Nature of the Chemical Bond. 3rd ed. Cornell Univ. Press, Ithica, N.Y., 88p.

Rappé, A.K., and Goddard III W.A. (1991) Charge equilibration for molecular dynamics calculations. Journal of Physical Chemistry, 95, 3358-3363.

Reddy, R. R., Ahammed, Y. N., Azeem, P. A., Gopal, K. R., & Rao, T. V. R. (2001). Electronic polarizability and optical basicity properties of oxide glasses through average electronegativity. J. Non-Cryst. Solids, 286, 169-180.

Retsinas, A., Kalampounias, A.G., and Papatheodorou, G.N. (2014) Reaching the ionic limit in the $(1-X)[Ca_{0.5}–Mg_{0.5}]O–XSiO_2$ pseudo-binary glass system with $0.5<X<0.27$: Glass formation and structure. Journal of Non-Crystalline Solids, 383, 38-43.

Richet, P., Mysen, B.O., and Andrault, D. (1996) Melting and premelting of silicates: Raman spectroscopy and X-ray diffraction of Li_2SiO_3 and Na_2SiO_3. Physics and Chemistry of Minerals, 23, 157-172.

Richet, P., Mysen, B.O., and Ingrin, J. (1998) High-temperature X-ray diffraction and Raman spectroscopy of diopside and pseudowollastonite. Physics and Chemistry of Minerals. 25, 401–414.

Richet, P, and Mysen, B.O. (1999) High-Temperature dynamics in cristobalite (SiO_2) and carnegieite ($NaAlSiO_4$): a Raman Spectroscopy study. Geophysical Research Letters, 26, 2283-2286.

Sawyer, R., Nesbitt, H.W., Bancroft, G.M., Thibault, Y., and Secco, R.A. (2015) Spectroscopic studies of oxygen speciation in K-silicate glasses and melts. Canadian Journal of Chemistry, 93, 60–73.

Sawyer, R., Nesbitt, H.W., and Secco, R.A. (2012) Three types of oxygen in K_2O-SiO^2 glasses: an X-ray photoelectron spectroscopy (XPS) study. Journal of Non-Crystalline Solids, 358, 290–302.

Shannon, R.D. (1976) Revised Effective Ionic Radii and Systematic Studies of Interatomie Distances in Halides and Chalcogenides. Acta Crystallographica, A32, 751-767.

Smith, R.P. (1956) The relationship of force constant and bond length. Journal of Physical Chemistry, 60, 1293-1296.

Smyth, J.R., and Hazen, R.M. (1973) The crystal structure of forsterite and hortonolite at several temperatures up to 900° C. American Mineralogist, 58, 588-593.

Spiekermann, G., Steele-MacInnis, M., Kowalski, P.M., Schmidt, C., and Jahn, S. (2013) Vibrational properties of silica species in $MgO–SiO_2$ glasses obtained from ab initio molecular dynamics. Chemical Geology, 346, 22-33.

Stixrude, L., and Karki, B. (2005) Structure and freezing of $MgSiO_3$ liquid in Earth's lower mantle. Science, 310, 297–299.

Swamy, V., Dubrovinsky, L.S., and Tutti, F. (1997) High-Temperature Raman Spectra and Thermal Expansion of Wollastonite. Journal of the American Ceramic Society, 80, 2237-2247.

Tomlinson, J.W., Hynes, M.S.R., and Bockris, J. O'M. (1958) The structure of liquid silicates. Part 2. – molar volumes and expansivities. Transactions of the Faraday Society, 54, 1822-1834.

Uchino, T., Iwasaki, M., Sakka, T., and Ogata, Y. (1991) Ab initio molecular orbital calculations on the electronic structure of sodium silicate glasses. Journal of Physical Chemistry, 95, 5455-5462.

Uchino, T., Sakka, T., Ogata, Y., and Iwasaki, M. (1992) Changes in the structure of alkali-metal silicate glasses with the type of network cation: Ab-initio molecular orbital study. Journal of Physical Chemistry, 96, 2455-2463.

Wang, A., Jolliff, B.L., Haskin, L.A. Kuebler, K.E., and Viskupic, K.M. (2001) Characterization and comparison of structural and compositional features of planetary quadrilateral pyroxenes by Raman spectroscopy. American Mineralogist, 86, 790-806.

Williams, Q., and Cooney, T.F. (1992) Cation field effects on orthosilicate glass vibrations. American Mineralogist, 77, 1-7.

Yamamoto, Y., Sawaguchi, N., and Sasaki, M. (2017) A new determination method of interatomic potential for sodium silicate glass calculations. Journal of Non-Crystalline Solids, 466-467, 29-36.

Zakaznova, V.P., Nesbitt, H.W., Bancroft, G.M., Tse, J.S., Gao, X., and Skinner, W. (2005) High-resolution valence-band XPS spectra of the non-conductors quartz and olivine. Physical Review B, 72, 205113 (1-13).

Zakaznova, V.P., Nesbitt, H.W., Bancroft, G.M., and Tse, J.S. (2008) Characterization of leached layers on olivine and pyroxenes using high-resolution XPS and density functional calculations. Geochimica et Cosmochimica Acta, 72, 69-86.

Zucker, R., and Shim, S.-H. (2009) In situ Raman spectroscopy of $MgSiO_3$ enstatite up to 1550 K. American Mineralogist, 94, 1638-1646.

Appendix

Optimized structures and their (harmonic) vibrational spectra were obtained from GAUSSIAN 03W, Version 6.1 (Frisch et al., 2004), with GAUSSVIEW 6.1 (Dennington et al., 2003) used as the user interface. The DFT method was used for the calculations with the 6-31G+(d):B3LYP basis set:functional combination. The detailed structure of this type of calculation varies with the particular basis set:functional used. Standard convergence criteria were used for the optimizations, and quadratically convergent SCF was used as needed. The latter does not change either the optimized structures found or their minimized energies or their vibrational spectra. The symmetries imposed on the optimizations are indicated in the text. None of the symmetry-restrained optimized structures are those that would be found if no symmetry were imposed, and therefore as expected, negative (imaginary) frequencies were found in the lower frequency range of the calculated vibrational spectra.

Mulliken charges are those for the optimized structures from the GAUSSIAN output. The Mulliken gross charge on an atom (Q_A) is related to "net" charge on an atom (Q_{AA}) by the formula (Mulliken 1955; Namba et al. 2003):

$$Q_A=Q_{AA}+1/2\Sigma Q_{AB} \quad (6)$$

and $1/2\Sigma Q_{AB}$ = the total overlap population.

Atoms in Molecules (AIM) charges which are based on in principle, observable electron densities (Bader, 2005), were calculated using the AIMAll suite of programs (Keith, 2016). Formatted checkpoint files for use as input for the AIMQB sub-program of AIMAll, were

obtained from standard checkpoint files outputted by GAUSSIAN via the FormChk utility of that program.

Table 1: Raman shifts (±2 cm^{-1}) of Q^2 crystals

Crystal	$\Omega(298)$ cm^{-1}	$\Omega(0)$	ω^* cm^{-1}	C	D	Pauling E.N.[f]
enstatite[a]	1025	1038	1048	-10.5	0	1.31
diopside[b]	1008	1010	1017	-7.27	-0.15	1.16[g]
wollastonite[c]	971	972.4	974.4	-5.75	0	1.00
p-wollastonite[b]	981	983	988	-4.94	-0.196	1.00
$Li_2SiO_3(c)$[b]	975	975	981	-4.08	-0.421	0.98
$Na_2SiO_3(c)$[b]	966	966	970	-3.96	-0.286	0.93
$K_2SiO_3(c)$[d]	963	~963	~971	?	?	0.82
$BaSiO_3(c)$[e]	964	?	?	?	?	0.89

a orthoenstatite from Zucker and Shim (2009).
b from Richet et al. (1996; 1998)
c from Swamy et al. (1997)
d from Brawer and White (1975)
e from Moulton et al. (2021)
f Pauling Electronegativities from Huheey et. al., (1997)
g electronegativity of diopside: Av. of Ca and Mg (not in fit)

Table 2: Q^2 Raman shifts at 298K for glasses (see references for uncertainties)

Glass Composition	Kal.[1] cm^{-1}	Ret.[2] cm^{-1}	B-W[3] cm^{-1}	Fur.[4] cm^{-1}	F&M[5] cm^{-1}	Ban.[6] cm^{-1}	O'Sh.[7] cm^{-1}	M-82[8] cm^{-1}	Av.Val. cm^{-1}	Electro-neg.[9]	M-O dist.[9]
$MgSiO_3$	990								**990**	1.31	0.1575
$CaMgSi_2O_6$		960						969	**965**		0.1441
$CaSiO_3$					950			963			0.1335
CaO=44.4%					955				**956**	1.00	0.1335
SrO= 44.4%					951				**951**	0.95	0.0982
BaO=44.4%					944						0.0808
BaO=46.1%								947	**946**	0.89	0.0808
$Li_2Si_2O_5$			950								
Li_2O=40%			955								
Li_2O=30%							950		**952**	0.98	0.2088
Na_2SiO_3					963			949			
Na_2O=40%			950	952							
Na_2O=30%							950				
$Na_2Si_2O_5$			945						**952**	0.93	0.1601
K_2O=40%			935								
K_2O=30%						943			**939**	0.82	0.1347
$Rb_2Si_2O_5$			935								
Rb_2O=30%							935		**935**	0.82	0.0993
$Cs_2Si_2O_5$			931								
Cs_2O=30%							931		**931**	0.79	0.0819

1 - Kalampounias (2009) - evaluated from their Fig. 3
2 - Retsinas et al. (2014) - evaluated from their Fig. 4
3 - Brawer and White (1975) from their Fig.4.
4 - Furukawa et al. (1981) - from their Fig. 5
5 - Frantz and Mysen (1995) from their Fig. 5 for $CaSiO_3$ and Fig. 9 for Na_2SiO_3.
6 - Bancroft et al. (2018) - from their Table 2
7 - O'Shaughnessy et al. (2020) - from their Tables
8 - Mysen et al. (1982) - from Figs. 4 to 7.
9 - Electronegativities and bond lengths: Huheey et al. (1997)

Table 3: Raman shifts and Si 2p3/2 BEs of some crystals and glasses

Phase	Composition	R. Shift cm^{-1}	Si $2p_{3/2}$ eV	O 1s(NBO) eV	O 1s(BO) eV	Reference[1]
Crist./Qz[2]	SiO_2	1200	103.6		532.8	5,6
Enstatite	$MgSiO_3$	1023	102.7	531.3	532.5	7,8
Diopside	$(CaMg)_{0.5}SiO_3$	1008	102.7	531.2	532.8	9,8
Forsterite	Mg_2SiO_4	856	101.7	531.0		10,6
Vit. Silica	SiO_2	1205	103.7		533.2	11,12
Q^3 of glass[3]	$Na_2Si_2O_5$	1091	102.0	532.0	530.0	13,12
Q^3 of glass[4]	$K_2Si_2O_5$	1098	101.8	529.7	531.9	14,15
Q^2 of glass	Na_2SiO_3	952	101.1	529.6	531.4	16,12

1 - 1st reference to the Raman shift and the 2nd is to the XPS values
2 - Raman shift is for cristobalite and Si 2p value is for quartz
3 - Raman shift is the average of Q^3 peak maxima of six Na-silicate glasses
4 - Q^3 peak maximum in a 30 mol% K-silicate glass
5 - Richet and Mysen (1999)
6 - Zakaznova-Herzog et al. (2005)
7 - Zucker and Shim (2009, Table 1) - Av. of n_{27} and n_{28} (site splitting)
8 - Zakaznova-Herzog et al. (2008)
9 - Richet et al. (1998)
10 - Chopelas (1991)
11 - Nesbitt et al. (2019)
12 - Nesbitt et al. (2011)
13 - Mysen et al. (1982)
14 - O'Shaughnessy et al. (2020)
15 - Sawyer et al. (2012)
16 - from Table 2

Table 4: Simulated properties for the $M_6Si_2O_7$ molecules

	$Li_6Si_2O_7$		$Na_6Si_2O_7$		$K_6Si_2O_7$	
	Eclipsed	Staggered	Eclipsed	Staggered	Eclipsed	Staggered
Bond lengths (Å)						
$Si-O_{NBO}$	1.662	1.662	1.667	1.666	1.667	1.664
$Si-O_{BO}$	1.635	1.633	1.653	1.649	1.673	1.668
$M-O_{NBO}$	1.843	1.845	2.166	2.174	2.493	2.515
M-Si	2.306	2.304	2.649	2.64	3.006	2.975
Bond angles						
$O_{NBO}-Si-O_{NBO}$	103.9	104.1	107.9	108.6	109.6	111.2
$O_{NBO}-Si-O_{BO}$	114.6	114.4	111.0	110.4	109.3	107.7
$O_{NBO}-M-O_{NBO}$	90.5	90.4	77.0	77.0	66.2	66.2
$M-O_{NBO}-M$	125.1	126.0	141.7	146.8	155.1	168.8
Mulliken charges						
Si	1.54	1.59	1.65	1.72	1.14	1.36
O_{NBO}	-0.93	-0.94	-1.25	-1.26	-1.18	-1.22
O_{BO}	-0.11	-0.20	-0.82	-0.91	-0.26	-0.55
M	0.44	0.44	0.83	0.84	0.85	0.87
AIM charges						
Si	3.19	3.19	3.17	3.17	3.16	3.16
O_{NBO}	-1.69	-1.69	-1.66	-1.67	-1.65	-1.65
O_{BO}	-1.66	-1.66	-1.66	-1.67	-1.68	-1.69
M	0.91	0.91	0.89	0.89	0.87	0.88
Raman shifts (cm^{-1})						
A band	901	902	852	859	833	828
Force constants (dynes/cm)						
	9.7E+05	9.7E+05	8.4E+05	8.4E+05	7.8E+05	7.6E+05
Reduced masses						
	20.2	20.2	19.5	19.5	19.0	18.8

Figure Captions:

Fig. 1: Temperature dependence of some Q^2 symmetric stretch frequencies for some metasilicate crystals. Enstatite (en) data are from Zucker and Shim, (2009), wollastonite (wo) from Swamy et al., (1997), diopside (di), pseudowollastonite (p-wo), Na_2SiO_3(c) and Li_2SiO_3(c) from Richet et al. (1996; 1998) and K_2SiO_3(c) from Brawer and White (1975). Uncertainties in Raman shifts are typically ±2 cm^{-1} but ±4 cm^{-1} where obtained from plots (see text and Nesbitt et al., 2018).

Fig. 2. The $M_2Si_2O_7$ molecule in eclipsed (a) and staggered (b) forms with symmetries indicated in brackets. Two silicon (Si) atoms center two tetrahedra with each Si bonded to one bridging oxygen (BO) atom and three non-bridging oxygen (NBO) atoms. There are six metal (M) atoms and each is bonded to *two* non-bridging oxygen (NBO) atoms as an attempt to mimic M atoms encased in O polyhedra of crystals, glasses and melts.

Fig. 3: Illustrates the relationship between Q^2 Raman shifts [Ω(298)] of alkali- and alkaline earth-bearing crystals and glasses versus electronegativities of the modifier metal oxide: (a) the crystals en, di, wo and p-wo (defined in Fig. 1), and Li = Li_2SiO_3(c), Na = Na_2SiO_3(c) and K = K_2SiO_3(c); (b) binary silicate glasses where the modifier oxide is indicated by its constituent metal. Sources of data are provided in the Tables. (c) Q^2 frequencies plotted against z/r^2 where r is the cationic radius (Huheey et al., 1997) for the most likely coordination number (CN). The solid bar associated with Ca illustrates the variation in z/r^2 with change in CN from 6 to 10 and is typical of variations in z/r^2 with CN for the cations plotted. Straight dashed lines are linear, least squares fits to the plotted data. Diopside and $Ca_{1/2}Mg_{1/2}SiO_3$ glass frequencies are plotted as open circles by taking average values for the abscissae (i.e., (Ca+Mg)/2) but they are not included in the fits

because the values for the abscissae cannot be rigorously assigned. R^2 values represent goodness-of-fit. See original references and Nesbitt et al. (2018) for uncertainties.

Fig. 4: Illustrates the relationship between alkali oxide (Na_2O and K_2O) content and BEs of Si 2p and O 1s core orbitals in Na and K silicate glasses. (a) diamonds and filled triangles represent O 1s BEs of BOs in K- and Na-silicate glasses; shaded and filled circles represent O 1s BEs of NBO in the same glasses. (b) Shaded and filled circles represent Si 2p BEs in K- and Na-silicate glasses. The solid lines are least squares best fits to Na-silicate data and the dashed lines are best fits to K-silicate data. The slope of each line is indicated by 'm' and R^2 represents goodness of fit. Error bars represent ±0.2 eV uncertainty in the measurements. Experimental data are from Nesbitt et al. (2011; 2017a, b) and Sawyer et al. (2012; 2015). Uncertainties are illustrated as bars.

Fig. 5. Illustrates the sympathetic decrease in Raman shifts and Si 2p BEs for Q species in numerous crystals and glasses containing progressively greater metal oxide contents. The solid symbols represent crystals and include cristobalite (crist.), enstatite (en), diopside (di) and forsterite (fo). The shaded circles represent glasses and include vitreous SiO_2, Q^3 of Na and K disilicate glasses and Q^2 of the Na metasilicate glass (data from Table 4). The solid and dashed curves are least squares best fits to the respective crystal and glass data. The partial charges on Si plotted at the top of the diagram are those of Namba et al. (2003). Uncertainties are large at typically ±30 cm^{-1}.

This is the peer-reviewed, final accepted version for American Mineralogist, published by the Mineralogical Society of America.
The published version is subject to change. Cite as Authors (Year) Title. American Mineralogist, in press.
DOI: https://doi.org/10.2138/am-2022-8172. http://www.minsocam.org/

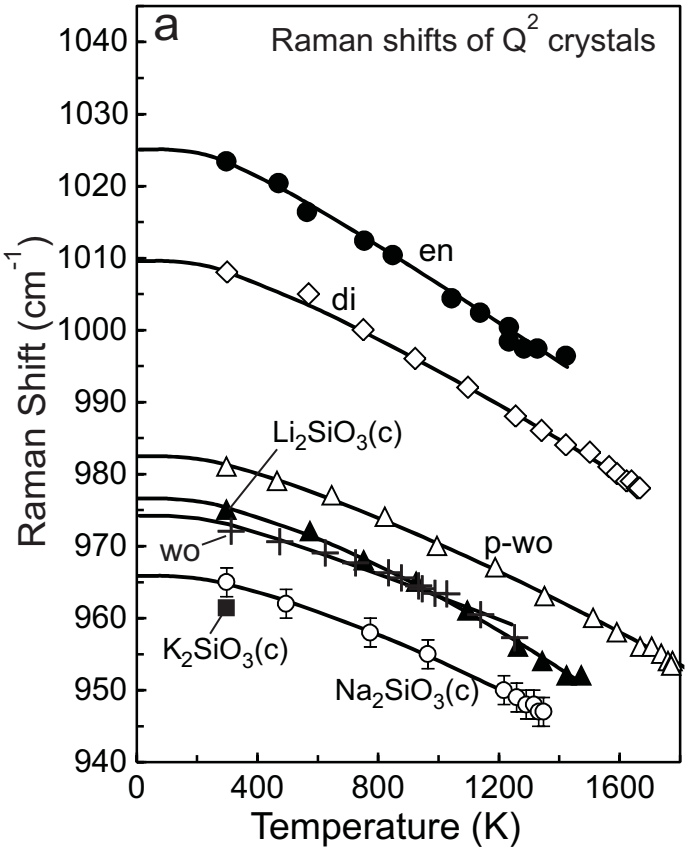

Fig. 1

This is the peer-reviewed, final accepted version for American Mineralogist, published by the Mineralogical Society of America.
The published version is subject to change. Cite as Authors (Year) Title. American Mineralogist, in press.
DOI: https://doi.org/10.2138/am-2022-8172. http://www.minsocam.org/

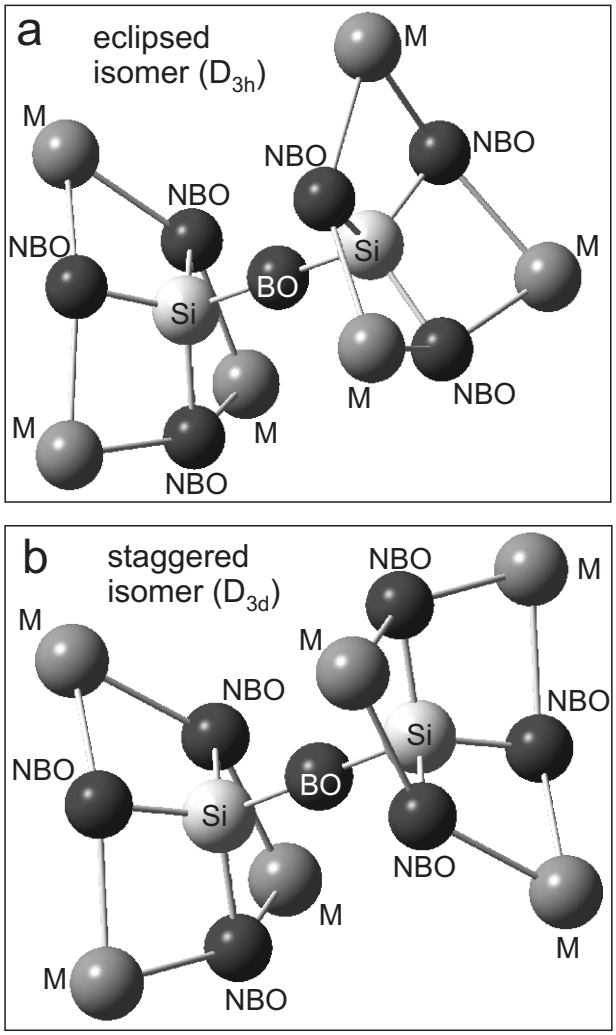

Fig. 2

This is the peer-reviewed, final accepted version for American Mineralogist, published by the Mineralogical Society of America.
The published version is subject to change. Cite as Authors (Year) Title. American Mineralogist, in press.
DOI: https://doi.org/10.2138/am-2022-8172. http://www.minsocam.org/

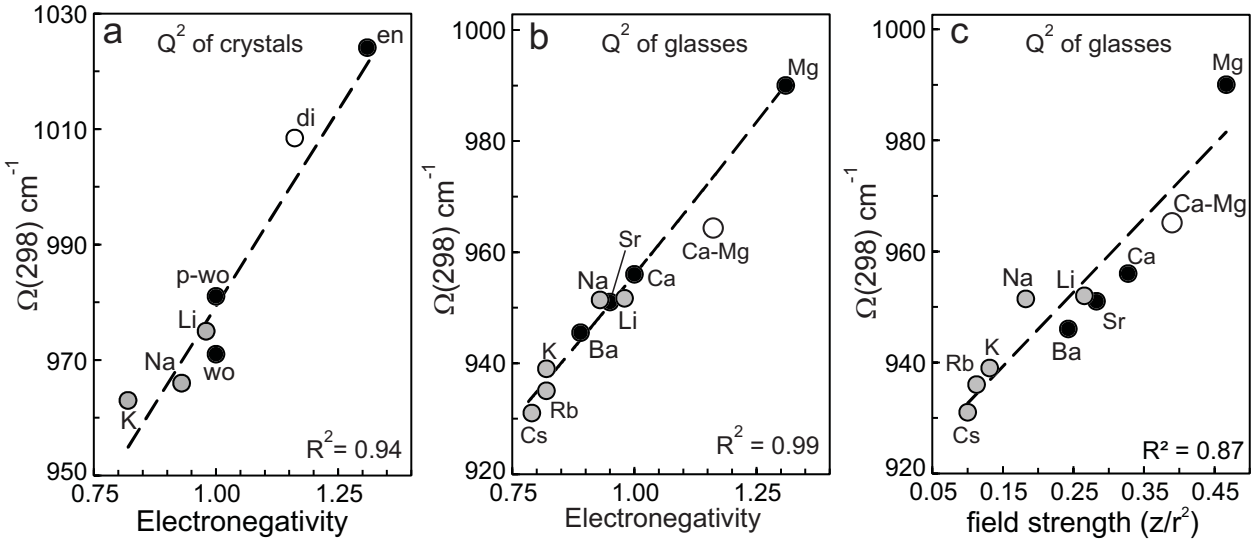

Fig. 3

This is the peer-reviewed, final accepted version for American Mineralogist, published by the Mineralogical Society of America.
The published version is subject to change. Cite as Authors (Year) Title. American Mineralogist, in press.
DOI: https://doi.org/10.2138/am-2022-8172. http://www.minsocam.org/

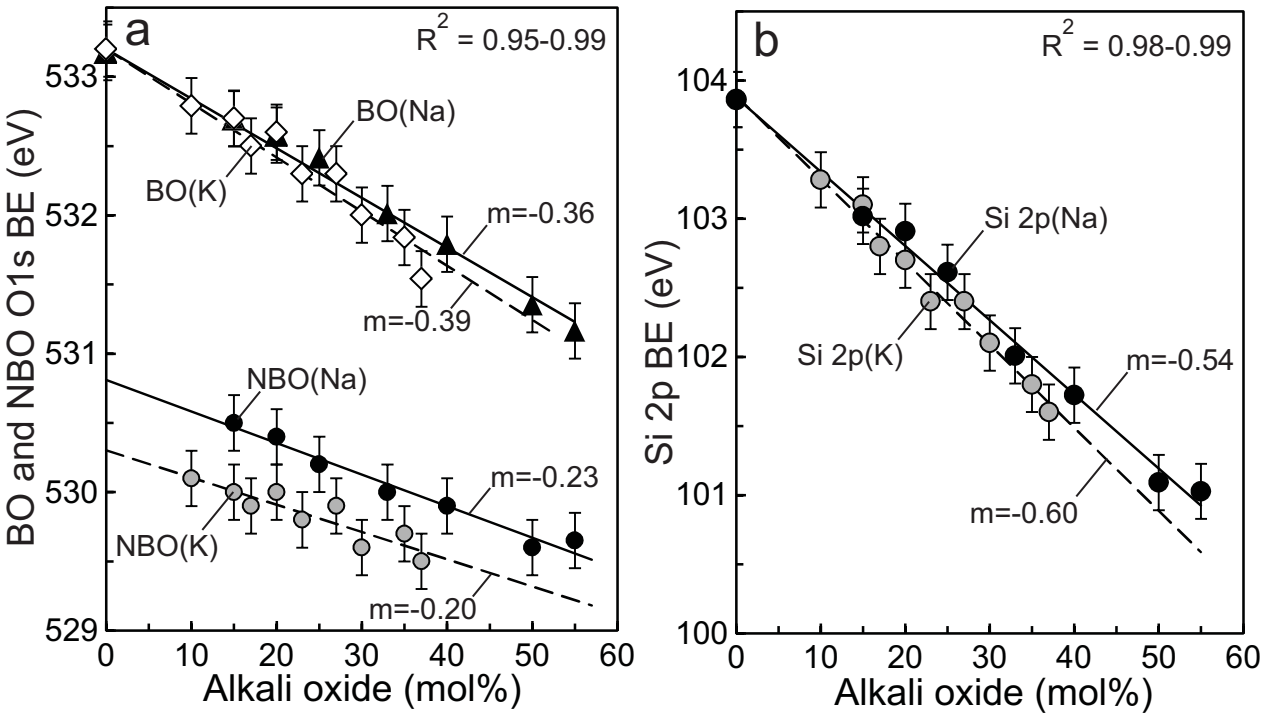

Fig. 4

This is the peer-reviewed, final accepted version for American Mineralogist, published by the Mineralogical Society of America.
The published version is subject to change. Cite as Authors (Year) Title. American Mineralogist, in press.
DOI: https://doi.org/10.2138/am-2022-8172. http://www.minsocam.org/

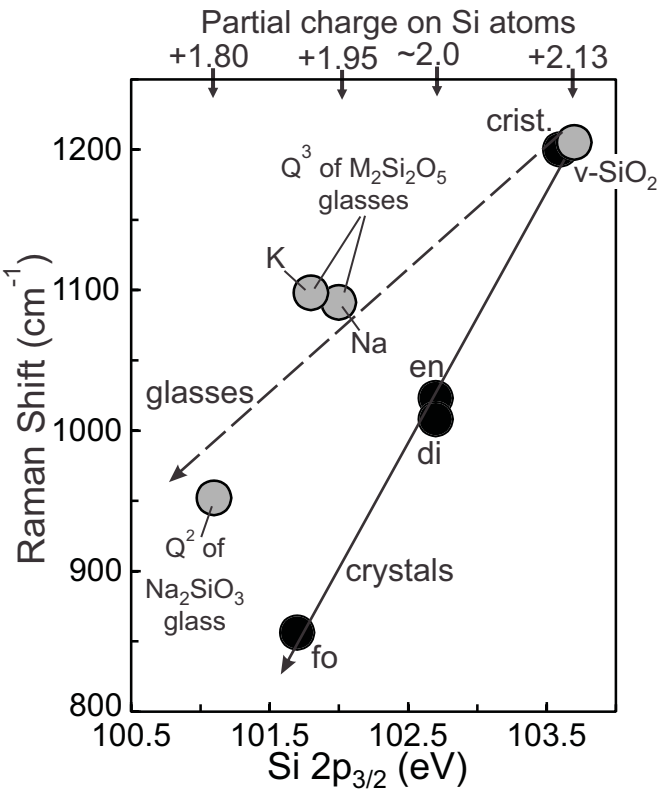

Fig. 5